Measurement of Molecular Diffusion in Solution by Multiphoton Fluorescence Photobleaching Recovery

Edward B. Brown,* En Shinn Wu,# Warren Zipfel,§ and Watt W. Webb§

*Department of Physics and §Department of Applied and Engineering Physics, Cornell University, Ithaca, New York 14853 and #Department of Physics, University of Maryland, Baltimore County, Baltimore, Maryland 21250 USA

ABSTRACT Multiphoton fluorescence photobleaching recovery (MP-FPR) is a technique for measuring the three-dimensional (3D) mobility of fluorescent molecules with 3D spatial resolution of a few microns. A brief, intense flash of mode-locked laser light pulses excites fluorescent molecules via multiphoton excitation in an ellipsoidal focal volume and photobleaches a fraction. Because multiphoton excitation of fluorophores is intrinsically confined to the high-intensity focal volume of the illuminating beam, the bleached region is restricted to a known, three-dimensionally defined volume. Fluorescence in this focal volume is measured with multiphoton excitation, using the attenuated laser beam to measure fluorescence recovery as fresh unbleached dye diffuses in. The time course of the fluorescence recovery signal after photobleaching can be analyzed to determine the diffusion coefficient of the fluorescent species. The mathematical formulas used to fit MP-FPR recovery curves and the techniques needed to properly utilize them to acquire the diffusion coefficients of fluorescently labeled molecules within cells are presented here. MP-FPR is demonstrated on calcein in RBL-2H3 cells, using an anomalous subdiffusion model, as well as in aqueous solutions of wild-type green fluorescent protein, yielding a diffusion coefficient of 8.7×10^{-7} cm^2s^{-1} in excellent agreement with the results of other techniques.

INTRODUCTION

Fluorescence photobleaching recovery (FPR) was introduced in the 1970s as a technique to measure the local mobility of fluorescently labeled particles bound to the plasma membrane of living cells (Peters et al., 1974; Axelrod et al., 1976; Edidin et al., 1976; Schlessinger et al., 1976; Cherry, 1979). It has since been used to study two-dimensional (2D) transport phenomena in a wide variety of biological membrane-bound systems. The 2D diffusional properties of aqueous systems are also accessible to conventional one-photon FPR, provided they are confined to a 2D diffusion geometry with thin samples or low numerical aperture (NA) optics (Henkel et al., 1996; Luby-Phelps et al., 1986; Johnson et al., 1996; Blonk et al., 1993). FPR has also been used to probe the photobleaching properties of fluorescent molecules confined in similar thin geometries (Periasamy et al., 1996).

This technique has been limited to the study of 2D diffusion because conventional one-photon excitation methods using focused laser beams generate fluorescence and photobleaching throughout extended, spreading, quasiconical regions of the sample above and below the focal plane. With one-photon excitation, the same amount of fluorescence signal and photobleaching is generated in each lateral plane along the optical axis, regardless of the distance from the focal plane (neglecting absorption losses along the optical axis). Thus the defined bleaching volume needed for an accurate FPR experiment previously has been achieved by intersecting the illumination beam with a thin sample constraining the fluorescent molecules of interest to 2D mobility, or by using low NA optics to generate an essentially cylindrical beam in a thick sample. These techniques yield an effective 2D diffusion coefficient of the fluorophore, where the diffusive properties of the fluorophore in the direction of the optical axis are lost. Furthermore, the measured 2D diffusion coefficient is an average over the thickness of the sample, with no three-dimensional (3D) resolution.

It has been claimed, without experimental evidence (Blonk et al., 1993), that one-photon excited photobleaching with confocal detection can yield the 3D diffusion coefficient of fluorophores with 3D resolution. We have evaluated this technique experimentally, and the results are discussed below.

The study of the diffusional mobility of fluorescent species has been extended into bulk fluid by a variety of techniques. Scanning microphotolysis (Wedekind et al., 1997) uses an intense focused laser beam to bleach continuously a solution of fluorescently labeled particles after a stepwise increase in intensity. The diffusion coefficient of the labeled particles is determined numerically by analyzing the approach to dynamic equilibrium of the fluorescence generated from unbleached molecules after the sudden onset of the bleaching beam. The excitation beam continuously causes photobleaching along the optical axis above and below the focal plane, so 3D resolution is only achieved by using confocal pinholes to confine the detection volume to the region of the focal point. This method produces a high signal-to-noise ratio because the fluorescence signal is be-

Received for publication 16 June 1998 and in final form 21 July 1999.

Address reprint requests to Dr. Watt W. Webb, Department of Applied and Engineering Physics, Cornell University, Clark Hall, Ithaca, NY 14853. Tel.: 607-255-3331; Fax: 607-255-7658; E-mail: browneb@msc.cornell.edu.

Dr. Edward Brown's present address is Edwin L. Steele Laboratory, Department of Radiation Oncology, Massachusetts General Hospital and Harvard Medical School, Boston, MA 02114 USA.

0006-3495/99/11/2837/13 $2.00

ing generated with an extremely intense laser beam and can be applied to any location within the sample (restricted to the sample depth accessible to confocal microscopy). However, the nonlocal nature of the photobleaching reduces the spatial resolution of the diffusion measurements, and the continuous high level of excitation may prove unhealthy for living tissue.

Total internal reflection fluorescence photobleaching recovery (TIR-FPR) (Swaminathan et al., 1996) uses the evanescent waves generated by total internal reflection of light from an interface between two materials of different indices of refraction (i.e., glass and water) as the excitation source for FPR experiments. The evanescent waves generated by TIR decay with increasing distance from the interface with the characteristic length scale of the wavelength of the excitation light. This restricts the photobleaching of fluorophores to regions close to the interface, thereby providing the three-dimensionally confined bleaching volume required by FPR. As a result of this restriction, TIR-FPR studies of cytoplasmic diffusion are possible only in regions of the sample within a few hundred nanometers of a water-glass interface, which generally limits this technique to the study of the immediate environment of the plasma membrane of cells directly attached to a coverslip.

Multiphoton fluorescence correlation spectroscopy (MP-FCS) (Berland et al., 1995; Mertz et al., 1995; Maiti et al., 1998) is a versatile technique using the intrinsic spatial confinement of fluorescence generated by multiphoton excitation to extend conventional FCS to bulk solutions. MP-FCS does not require photobleaching of the fluorescent label and can be performed anywhere in the bulk cytoplasm of a living cell within thick tissue samples. This technique is limited, however, to low concentrations (typically nanomolar) of fluorescent molecules.

Multiphoton excitation (MPE) offers an ideal pathway for the extension of conventional FPR techniques into the bulk cytoplasm (Piston et al., 1992; Svoboda et al., 1996). In the absence of excitation saturation, the rate of excitation per molecule undergoing m-photon excitation (where m can be 1, 2, 3, etc.) is

$$\text{Rate} \equiv (1/m)\delta_m\langle I^m\rangle \quad (1)$$

where δ_m is the multiphoton absorption cross section in units of $cm^{2m}s^{m-1}$ $photon^{m-1}$ and $\langle I^m\rangle$ is the time average of the mth power of the local intensity, in units of photons $s^{-1}cm^{-2}$. Under nonsaturating conditions, the dependence of MPE on the second or higher power of the intensity gives the technique an intrinsic 3D resolution, with $\geq$80% of the excitation confined to the e^{-2} isointensity surfaces of the focused laser intensity distribution (Denk et al., 1995). Using MPE with a uniformly illuminated high numerical aperture (NA) objective, fluorescence excitation and, therefore, photobleaching can be confined to less than femtoliter volumes, with $\sim$1 μm resolution along the laser propagation axis.

In a MP-FPR experiment, a brief, intense pulse train from a mode-locked laser bleaches a small volume of fluorescently labeled particles within a larger solution via multiphoton excitation. The attenuated laser then generates fluorescence as unbleached fluorophores diffuse into the focal volume from the surrounding environment. The resultant fluorescence recovery curve has an amplitude proportional to the initial local bleaching of the fluorophore and a duration that depends upon the local diffusion coefficient of the labeled particle. MP-FPR can determine the mobility properties of fluorescently labeled molecules or particles throughout the cytosol of cells even deep within thick tissue samples, at higher fluorophore concentrations than MP-FCS and without generating the large quantities of photobleaching byproducts that occur with scanning microphotolysis. While the spatial scale of the bleached distribution generated with typical excitation wavelengths and objective lenses is $\sim$1 μm, the formation of a fluorescence recovery curve depends upon the inward diffusion of unbleached fluorophore from outside the bleached distribution, giving MP-FPR a spatial resolution of a few microns.

In this publication we present a user's guide to this new technique and demonstrate its use. The Materials and Methods section details the equipment that is necessary for MP-FPR capabilities to be added to a conventional multiphoton laser scanning microscope, and the derivations of the formulae that are used to fit MP-FPR curves for the determination of diffusion coefficients are presented in the Theoretical Results. The results of the demonstration of MP-FPR on the known diffusion coefficient of wild-type green fluorescent protein (wtGFP) are presented in the In Vitro Demonstration Experiment section, and the results of the demonstration of MP-FPR's applicability in living cells is presented in the In Vivo Demonstration Experiment section. The validity of a competing one-photon confocal FPR technique in the determination of 3D diffusion coefficients with 3D resolution is detailed in the Discussion. The primary sources of systematic and random error in MP-FPR are also reviewed in the Discussion.

MATERIALS AND METHODS

Experimental apparatus

In these experiments MP-FPR was accomplished with a tunable mode-locked Ti:sapphire laser (Tsunami; Spectra Physics, Mountain View, CA) that produces $\sim$80-fs pulses at a repetition rate of 80 MHz. The beam was rapidly modulated by a KDP* Pockels Cell (model 350-50; Conoptics, Danbury, CT) to generate the bleaching and monitoring intensities. A 5$\times$ beam expander ensured proper overfilling of the back aperture of the microscope objective (1.3 NA, 40$\times$ oil immersion; Zeiss, Jena, Germany), which focused the excitation light on a fluorescent sample (see Fig. 1). For all experiments the objective lens was overfilled, which we define as occurring when the e^{-1} radius of the excitation beam is greater than or equal to the radius of the objective back aperture (the entrance pupil). Calculations have shown that with an e^{-1} beam radius equal to the radius of the back aperture there is less than a 6% deviation from the true diffraction-limited case (W. R. Zipfel, unpublished calculations). A pair of SF10 prisms in the excitation beam path was used to compensate for the group delay dispersion of the optical components.

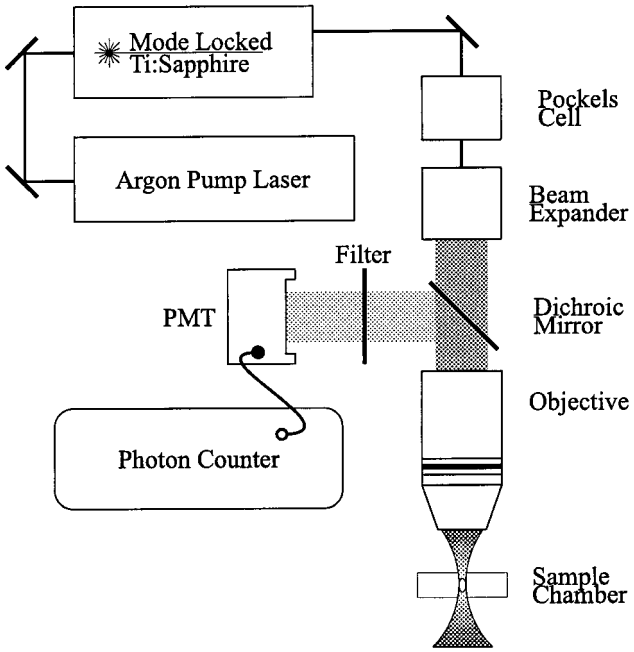

FIGURE 1 Equipment diagram. This is the apparatus used for the in vitro study of the diffusion coefficient of wild-type GFP in solution. The in vivo experiments discussed in this work also included a laser scanning system to image the sample before photobleaching.

Fluorescent samples (4.4 μM wild-type GFP in pH 8 Tris-HCl buffer; Clonetech, Palo Alto, CA) were held in deep well slides (~500-μm well depth) beneath no. 1.5 coverslips positioned such that the multiphoton focal volume generated by the objective was within the fluorescent solution but close to the coverslip (within ~10 μm), to minimize aberrations due to the mismatch between the index of refraction of the oil immersion lens and the aqueous solution. These aberrations can cause the size of the focal volume to increase with the distance between the focal point and the coverslip. In typical physiological applications of MP-FPR involving water immersion objective lenses with or without coverslips, these aberrations will not be a significant problem. Fluorescence was separated from the excitation light path by a 650-nm long-pass dichroic mirror (650 LP; Chroma Technologies, Brattleboro, VT) and three 550 DF 150 bandpass filters (550 DF 150; Chroma Technologies). This fluorescence was monitored using a photomultiplier tube (HC-125-02; Hammamatsu, Bridgewater, NJ) connected to a zero dead-time photon counter (SR430; Stanford Research Systems, Sunnyvale, CA). Resonances in the KDP* Pockels Cell cause some ~17 μs damped oscillations in the transmittance of the Pockels Cell after the brief bleaching pulse, which can lead to systematic errors when diffusion coefficients greater than 10^{-7} cm^2s^{-1} are measured. These oscillations were quantified using the excitation light reflected from the dichroic mirror with another photomultiplier tube and photon counter arrangement. The fluorescence signal was then divided by the square of this reference signal, eliminating the oscillations from the data. To reduce shot noise in the wtGFP data, the pulse-monitoring procedure was repeated 10,000 times at a rate (20 Hz) slow enough to allow diffusional replenishment of the two-photon focal volume between repetitions.

The $1/e^2$ axial dimension of the excitation beam was verified by scanning the focal spot across the interface between a fluorescent dye and the coverslip. Using the appropriate ellipsoidal Gaussian approximations (as described below) to the exact form of the diffraction limited intensity, we calculated the radial e^{-2} dimension. For this work a radial dimension of 0.248 μm and an axial dimension of 0.860 μm were used to describe the two-photon focal volume produced by overfilling a 1.3 NA objective lens with 780-nm light.

In vivo experiments

RBL-2H3 cells were grown in stationary culture and harvested by incubation for 15 min in calcium-chelating buffered salt solution (135 mM NaCl, 5 mM KCl, 20 mM HEPES, and 1.5 mM EDTA at pH 7.4). Released cells were centrifuged at 1000 rpm for 8 min, resuspended in the original culture medium, placed in 35-mm coverslip-bottomed microwells (MatTek Corp., Ashland, MA) at 2×10^5 cells per well, and allowed to adhere overnight at 37°C in a 5% CO_2 incubator. Cells were loaded by incubation with 1 μM Calcein Green-AM (Molecular Probes, Eugene, OR) for 5 min, rinsed twice, and then immersed in 1 ml of HEPES-buffered salt solution (135 mM NaCl, 1.8 mM $CaCl_2$, 5 mM KCl, 1 mM $MgCl_2$, 20 mM HEPES, 5 mM glucose, and 0.1% gelatin at pH 7.4). The in vivo data were acquired on a lab-built laser-scanning multiphoton microscope utilizing a Bio-Rad scanner (Bio-Rad, Hemel Hempstead, England) and an Olympus BX50WI upright microscope (Olympus, Melville, NY). The beam modulation and signal detection apparatus were identical to the in vitro apparatus. Calcein-loaded cells were located by imaging with the microscope, and MP-FPR was carried out by parking the laser beam at the desired position within the cell. Fifty bleach/monitor repetitions were performed at a rate (5 Hz) slow enough to allow replenishment of the focal volume between bleaches. An Olympus 1.35 NA oil immersion lens was used. The e^{-2} radii in the lateral and axial dimensions were calculated to be 0.237 μm and 0.822 μm, respectively, under 780-nm excitation.

Data analysis

The data generated with this technique were fit to the fluorescent recovery curves derived in the following section, yielding the diffusion coefficient of the fluorescent diffusing molecules. The fitting routine uses the Levenberg-Marquardt algorithm (Press et al., 1992) and is available at http://www.englib.cornell.edu/drbio/fpr.html.

THEORETICAL RESULTS

In an MP-FPR experiment, a pulse train of high-intensity laser illumination photobleaches a fraction of fluorescent particles in a small volume within a solution. The photochemical mechanisms of photobleaching are not completely understood and are the subject of ongoing research under both one-photon (Song et al., 1995, 1996; Kasche and Lindqvist, 1964) and multiphoton (Xu and Webb, 1997) excitation, often using FPR techniques. For this research we define photobleaching as the transition of a fluorophore to a nonfluorescent state with a lifetime significantly longer than the diffusive recovery time of the experimental system. In the simplest model of photobleaching, the multiphoton bleaching of molecular fluorophores is described by a first-order differential equation,

$$\frac{dc(r, z, t)}{dt} = -(1/b)q_b\delta_b\langle I_{bl}^b(r, z)\rangle c(r, z, t) \qquad (2)$$

where we have used the notation of Eq. 1 with $m \rightarrow b$ for bleaching. The multiphoton absorption cross section of the fluorophore for the order of excitation responsible for the bleaching of the fluorophore is δ_b, and q_b is the quantum efficiency for b-photon photobleaching. The time average of the bleaching intensity raised to the bth power is $\langle I_{bl}^b(r, z)\rangle$, where b is the number of photons absorbed in a bleaching event. Equation 2 assumes that there is no satu-

ration of the fluorescence excitation process, which means that only a small fraction of the fluorophores at any location in the focal volume are excited with each laser pulse. For a bleaching pulse train of duration Δt that is much shorter than the diffusion time of the fluorescently labeled particle, the solution of Eq. 2 yields the concentration distribution of unbleached fluorophore at the end of the bleaching pulse train,

$$c(r, z, t = \Delta t) = c_0 \exp[-(1/b) q_b \delta_b \langle I_{bl}^b(r, z)\rangle \Delta t] \quad (3)$$

where c_0 is the initial equilibrium concentration of fluorophore.

The mathematical form of the diffraction-limited intensity distribution is too complex for convenient analytical solutions of the MP-FPR fluorescence recovery curve. However, the nonlinear dependence of multiphoton excitation on laser intensity reduces the excitation generated by secondary peaks relative to the central peak, and for two- or higher-order excitation the effective excitation intensity distribution can be modeled using a 3D Gaussian approximation:

$$\langle I_{bl}^b(r, z)\rangle = \langle I_{bl}^b(0, 0)\rangle \exp\left[-\frac{2br^2}{w_r^2} - \frac{2bz^2}{w_z^2}\right] \quad (4)$$

where w_r and w_z are the e^{-2} radial and axial dimensions, respectively, and $\langle I_{bl}^b(0, 0)\rangle$ is the time average of the intensity at the center ($r = z = 0$) of the two-photon focal volume raised to the bth power. When b is 2 or higher, this expression can be used as the laser intensity profile in Eq. 3 with the necessary degree of accuracy to fit experimental data. The nonequilibrium distribution of unbleached fluorophore immediately after the photolysis pulse train (Eqs. 3 and 4) can be propagated forward in time during the fluorescence recovery via solution of the diffusion equation in integral form, yielding the time-dependent fluorophore concentration distribution $c(r, z, t)$ (see the Appendix). If we illuminate the bleached distribution of dye with a weak monitoring beam (generally the attenuated bleaching beam) and generate fluorescent photons by an m-photon process, the fluorescence intensity detected is given by

$$F(t) = (1/m) E \delta_m \int \langle I_{mo}^m(r, z)\rangle c(r, z, t) 2\pi r \, dr \, dz \quad (5)$$

where m is the number of photons required to generate a fluorescence photon, δ_m is the fluorescence action cross section of the fluorophore undergoing m-photon excitation, E is the overall efficiency of the detection system, and $\langle I_{mo}^m(r, z)\rangle$ is the time average of the mth power of the intensity of the monitoring beam at position r and z. The application of Eq. 5 to the appropriate time-dependent fluorophore concentration is shown in the Appendix, and the resultant solution for time-dependent fluorescence signal after the photobleaching pulse train is given by

$$F(t) = F_0 \sum_{n=0}^{\infty} \frac{m^{3/2}(-\beta)^n}{n!} \frac{1}{(m + bn + (bnmt/\tau_D))} \times \frac{1}{\sqrt{m + bn + (bnmt/(R\tau_D))}} \quad (6)$$

where D is the diffusion coefficient of the fluorophore and the characteristic radial diffusion time of the fluorophore through the multiphoton focal volume is $\tau_D \equiv w_r^2/8D$. The prebleach equilibrium fluorescence signal is F_0, and $R \equiv w_z^2/w_r^2$ is the square of the ratio of the $1/e^2$ beam dimensions, which means that the characteristic axial diffusion time of the fluorophore through the multiphoton focal volume is $R\tau_D$. The bleach depth parameter β (alternatively, the "bleaching dose") is defined as $\beta \equiv (1/b) q_b \delta_b \langle I_{bl}^b(0, 0)\rangle \Delta t$ and contains the bleaching action cross section $q_b\delta_b$, the time average of the peak intensity at the center of the focal spot raised to the bth power, and Δt, the duration of the bleaching pulse train.

The influence of various experimental parameters upon the behavior of the fluorescence recovery curve can be understood in terms of the bleach depth and the initial slope of the recovery. The bleach depth ΔF, which is defined as $[F_0 - F(t = 0)]/F_0$, is not equal to the bleach depth parameter β. Inspection of Eq. 6 reveals that the two are related as follows:

$$\Delta F = \frac{F_0 - F(t = 0)}{F_0} = 1 - \sum_{n=0}^{\infty} \frac{(-\beta)^n}{n!} \frac{1}{(1 + (bn/m))^{3/2}} \quad (7)$$

which is plotted in Fig. 2 *A* with $m = b$. For small values of the bleach depth parameter, the bleach depth scales linearly with β, and consequently it scales linearly with the duration of the photobleaching flash and with the bth power of the bleaching intensity. At deeper bleaches, as the fraction of bleached fluorophore in the center of the focal volume approaches 1, the bleach depth no longer scales linearly with β.

The initial slope of the recovery curve is given by

$$\frac{\partial F(t)}{\partial t} = -\frac{F_0}{\tau_D}\left(\frac{1}{2R} + 1\right) b \left[\sum_{n=0}^{\infty} \frac{(-\beta)^n}{n!} \frac{n}{(1 + (bn/m))^{5/2}}\right] \quad (8)$$

and the term contained in square brackets is plotted in Fig. 2 *B* with $m = b$. This initial slope is positive, scales linearly with D (i.e., inversely with τ_D), and increases with increasing β. This initial slope of the fluorescence recovery curve is dominated by the diffusive recovery in the radial dimension, with a time scale of τ_D. If the NA of the excitation optics is decreased, making the focal spot more elongated (i.e., making R larger), the axial profile of the focal volume (as represented by the value of R) becomes less significant in defining the initial slope of the recovery curve. In the limit that $R \gg 1/2$ (the minimum value of R in aqueous solution is ~3, for a 1.33 NA lens) the value of R and therefore the axial profile do not influence the initial slope

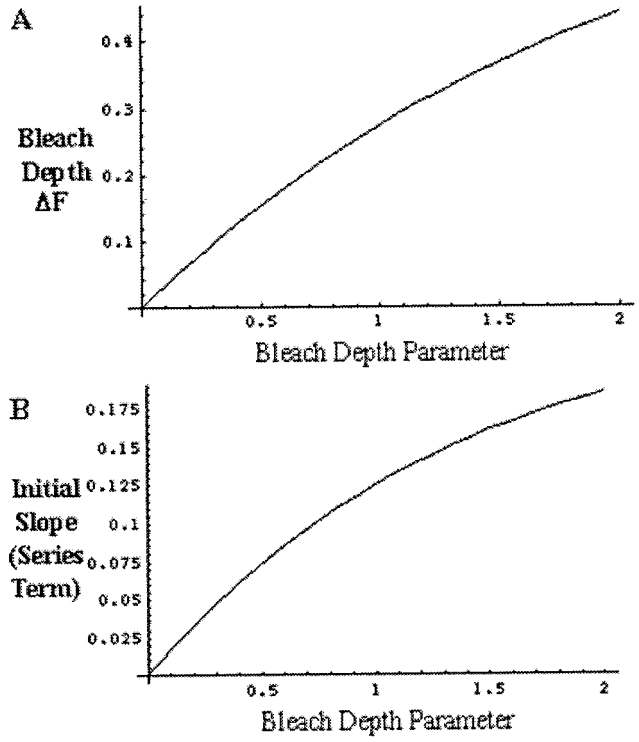

FIGURE 2 (*A*) Dependence of the bleach depth $(F_0 - F(t = 0))/F_0$ on the bleach depth parameter β for $m = b$, as shown in Eq. 7. (*B*) Dependence of the initial slope of the recovery curve on the bleach depth parameter β for $m = b$, as shown in Eq. 8. The quantity plotted is

$$\left.\frac{\partial F(t)}{\partial t}\right|_{t=0} \times \frac{\tau_D}{F_0((1/2R) + 1)b}$$

of the recovery curve at all. Greater bleach depths, represented by greater values of β, produce steeper initial slopes of the fluorescence recovery curve. This is because at higher bleach depths the initial unbleached fluorophore distribution given by Eq. 3 begins to approach an inverted top-hat shape as essentially all of the fluorophore is bleached out at the center of the focal volume. The steeper gradient of unbleached fluorophore at the edges of this top-hat shape results in more rapid initial diffusive recovery immediately after the bleach pulse.

The experimental validity of the ellipsoidal Gaussian approximation to the multiphoton focal volume was evaluated by numerically generating fluorescence recovery curves using the full expression for the diffraction-limited intensity distribution (Born and Wolf, 1983). These pseudo-data curves were then fit to Eq. 6, and the accuracy of the resultant diffusion coefficient was evaluated. The error due to the ellipsoidal Gaussian approximation is less than 6% for values of β between 0 and 5.

The series solution for the one-photon, 2D FPR geometry analogous to Eq. 6 can be linearized for small values of β (Yguerabide et al., 1982), allowing appropriately transformed data to be rapidly fit to a straight line. This linearization is problematic in the multiphoton, 3D case because of the square root term in the denominator of Eq. 6. We see from Eqs. 7 and 8 that in the limit of small β, the MP-FPR recovery curve has a $t = 0$ intercept of $\Delta F = (2^{-3/2}\beta)$ and a $t = 0$ slope of

$$\left.\frac{\partial F(t)}{\partial t}\right|_{t=0} = \frac{F_0}{\tau_D}\left(\frac{1}{2R} + 1\right)\frac{\beta}{2^{5/2}} \quad (9)$$

which may prove useful for rapid fitting estimates.

In vitro MP-FPR demonstration

In this experiment a solution of wild-type GFP diluted to 4.4 μM in water was photobleached with a 7.2-μs pulse train of 780 nm light overfilling a 1.3-NA objective, and the resultant fluorescence recovery curve was monitored with 10.24-μs time bins. This value of the pulse train duration was short enough to avoid significant fluorophore diffusion during the photobleaching flash, while the value of the time bin duration was found to avoid significant fluorophore diffusion during a single time bin and therefore to allow accurate recording of recovery curve. To determine appropriate levels of the average photobleaching power, the bleach depth parameter at a variety of average photobleaching powers was measured; the results are shown in Fig. 3. At bleaching powers below ~44 mW at the sample (marked by the *vertical line* in Fig. 3) the bleach depth parameter was found to scale as the bleaching power squared, and Eq. 2 was therefore valid in this range with $b = 2$. At higher bleach powers the system underwent excitation saturation (as discussed below), and Eq. 2 was no longer valid. The bleaching power was therefore restricted to values less than ~44 mW for the following experiment.

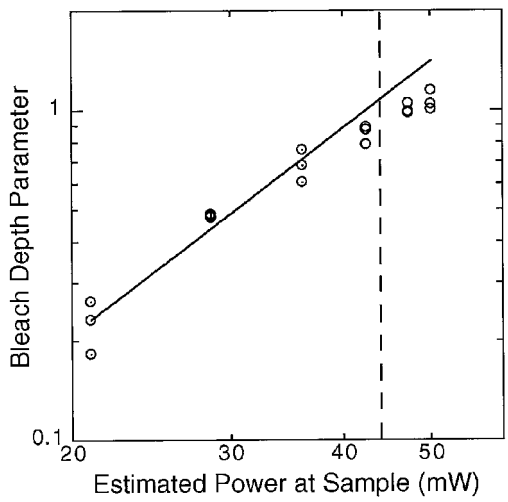

FIGURE 3 Saturation of wild-type GFP photobleaching. Data were taken with 7.2-μs pulse trains of 780 nm light overfilling a 1.3-NA objective. Excitation saturation causes the bleach depth parameter to lose its power squared dependence (line slope = 2.1), as a significant fraction of the fluorophores at the center of the focal volume are excited by each laser pulse. The vertical line marks the apparent onset of saturation and corresponds to a value of $s = \frac{1}{2}g_p^{(2)}\delta\langle I_{bl}(0, 0)\rangle^2\omega^{-2}\tau^{-1}$ of ~1.

A sample bleaching recovery curve with the corresponding fit using Eq. 6 is shown in Fig. 4. The average bleaching and monitoring powers were ~19 mW and ~1 mW at the sample. This value of the average monitoring power was found to avoid significant photobleaching during the monitoring phase, as measured by the average loss of signal during a scan in the absence of a photobleaching flash. The extremely low concentration of fluorophore required the summation of 10,000 consecutive pulse/monitor sequences to yield the curve shown. The equilibrium fluorescence signal and the bleach depth both scaled with the square of the excitation power; therefore $m = b = 2$ in Eq. 6. The calculated diffusion coefficient for wild-type GFP determined from 22 similar MP-FPR curves is $8.7 \times 10^{-7} \pm 1.7 \times 10^{-7}$ cm^2s^{-1}. This agreed with the value of 8.7×10^{-7} cm^2s^{-1} derived from conventional FPR experiments on the S65T mutant of GFP (Swaminathan et al., 1997). The diffusion coefficient for aqueous solutions of wild-type GFP showed no tendency to vary with bleaching depth when measured at various bleaching intensities, corresponding to values of β up to 0.7 and average bleaching powers at the sample up to ~24 mW.

In vivo MP-FPR demonstration

An in vivo MP-FPR experiment using calcein-AM-loaded RBL cells yielded the recovery curve showed in Fig. 5 *A*. MP-FPR was performed with 780 nm light overfilling a 1.35-NA objective. A 20-μs bleaching pulse of ~10 mW at the sample, with ~0.3 mW at the sample for a monitoring beam, 10.24-μs time bins, and an average of 50 pulse-monitor sequences, yielded the recovery curve shown. These values of the bleaching and monitoring power were found to avoid saturation and significant photobleaching, respectively, while the values of the bleaching duration and time bin duration were rapid enough to avoid significant diffusional recovery during the given interval. The MP-FPR curve from an in vitro MP-FPR experiment on calcein in water is also shown in Fig. 5 *B* for comparison.

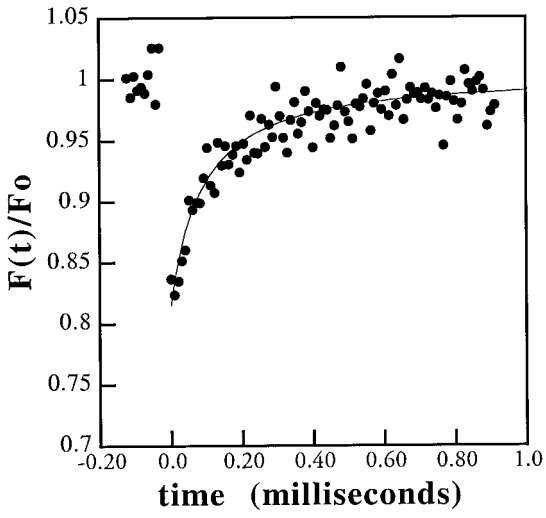

FIGURE 4 Fluorescence recovery curve of 4.4 μM aqueous solution of wild-type GFP. Photobleaching was accomplished with a 7.2-μs pulse train of 780 nm light overfilling a 1.3-NA objective. The bleach power was ~19 mW at the sample, and the monitoring power was ~1 mW at the sample, yielding an average accumulated count per bin of $F_0 \approx 25{,}000$. Using r and z $1/e^2$ radii of 0.248 μm and 0.860 μm, respectively, a bleach depth parameter of 0.61 and a diffusion coefficient of 8.8×10^{-7} cm^2/s produced the fit shown.

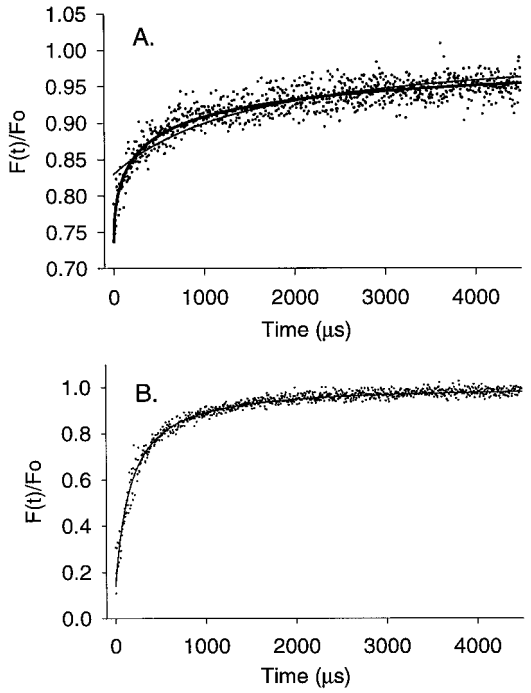

FIGURE 5 (*A*) Fluorescence recovery curve of AM-loaded calcein in an RBL cell (internal concentration is ~100 μM) and (*B*) 30 μM calcein in solution. Photobleaching was accomplished with a 20-μs bleaching pulse train of 780 nm light overfilling a 1.35-NA objective. The bleach power was ~10 mW at the sample, and the monitoring power was ~0.3 mW at the sample. Fifty flash-monitor sequences were averaged to yield the data shown. An adaptation of Eq. 6 that includes anomalous subdiffusion (Feder et al., 1996) was used to fit the data in *A* (best fit line), yielding an anomalous subdiffusion parameter of $\alpha = 0.55$, and a time-dependent diffusion coefficient; $D(10\ \mu s) = 1.2 \times 10^{-6}$ cm^2s^{-1}, $D(6\ ms) = 7.0 \times 10^{-8}$ cm^2s^{-1}. The additional solid line shown in *A* (poorer fit) is the result of fitting the data to a single diffusion coefficient model (Eq. 6). Data in *B* were fit to the MP-FPR expression (Eq. 6), resulting in a diffusion coefficient of 1.5×10^{-6} cm^2/s.

We find that in vivo MMP-FPR curves of calcein in RBL-2H3 cells typically require a more complicated treatment than the free diffusion model with one diffusing component that resulted in Eq. 6 (see Fig. 5 *A*). Application of Eq. 6 to in vivo data poorly fits the early time behavior of the fluorescence recovery and requires a large immobile fraction (see the Discussion). This is problematic because the MP-FPR curves were generated by 50 bleaching flashes at the same spot, suggesting that any immobile fraction would be thoroughly bleached out. These complications contrast with the in vitro MP-FPR curves of calcein in water, where the fluorescence recovery is well fitted with the conventional diffusion model described by Eq. 6, with

no immobile fraction (Fig. 5 *B*). To analyze the in vivo fluorescence recovery curves of calcein we considered two models, an anomalous subdiffusion model, and a weighted sum of two diffusion terms.

The anomalous subdiffusion model was first observed in cell surface diffusion (Ghosh and Webb, 1988) and studied and analyzed by Feder et al. (1996) and Perisamy and Verkman (1998). It assumes that the presence of potential energy traps causes the mean square displacement of a diffusing particle to obey a power law in time (Bouchard and Georges, 1990):

$$\langle r^2 \rangle = 4D(t)t = 4\Gamma t^{\alpha} \tag{10}$$

where α is the anomalous diffusion parameter that measures the extent to which diffusive motion is retarded by the environment, and Γ is a constant "transport coefficient." This expression reduces to conventional free diffusion as α approaches 1. Mathematically this model is applied to MP-FPR experiments by modifying Eq. 6, replacing terms of the form Dt with terms of the form $(Dt)^{\alpha}$ (Feder et al., 1996; Perisamy and Verkman, 1998). In this model the fitting parameter D does not have units of cm^2s^{-1}. The effective diffusion coefficient at any time t is then equal to $D^{\alpha}t^{\alpha-1}$. Analysis of the data revealed that no immobile fraction was needed to improve the quality of the fit. This results in a three-parameter fit (β, α, D).

An alternative treatment of complex diffusion data assumes multiple diffusion coefficients (Perisamy and Verkman, 1998). This model is applied to MP-FPR experiments by fitting fluorescence recovery curves to a weighted sum of two conventional MP-FPR curves with $m = b = 2$:

$$\frac{F(t)}{F_0} = A_1\left[\sum_{n=0}^{\infty}\frac{(-\beta)^n}{n!}\frac{1}{(1+n+2nt/\tau_{D_1})}\frac{1}{\sqrt{1+n+2nt/(R\tau_{D_1})}}\right] + A_2\left[\sum_{n=0}^{\infty}\frac{(-\beta)^n}{n!}\frac{1}{(1+n+2nt/\tau_{D_2})}\frac{1}{\sqrt{1+n+2nt/(R\tau_{D_2})}}\right] \tag{11}$$

where A_1 and A_2 are the relative contributions of the two diffusing components to the fluorescence recovery signal and τ_{D_1} and τ_{D_2} are two independent diffusional recovery times. Analysis of the data revealed that no immobile fraction was needed to significantly improve the fit to the data, so A_1 and A_2 were constrained to add to 1. This results in a four-parameter fit (A_1, D_1, D_2, β).

We applied both models to in vivo MP-FPR data of calcein in the cytoplasm of RBL-2H3 cells. The fits produced by both models are far superior to the conventional free diffusion model with one diffusion coefficient. The diffusion coefficients reported by the multiple diffusion coefficient model are strongly influenced by the length of the data set relative to the diffusive recovery time, while the anomalous subdiffusion fit is insensitive to this parameter. Furthermore, the multiple diffusion coefficient model does not fit the earliest, deepest fluorescence data points as well as the anomalous subdiffusion model. Last, the diffusion coefficients reported by the multiple diffusion coefficient model exhibit a much greater variability than the anomalous subdiffusion model, with relative uncertainties as great as 120%. We therefore chose to analyze our in vivo MP-FPR data with the anomalous subdiffusion model.

Analysis of MP-FPR curves from the cytoplasm of three RBL-2H3 cells using the aforementioned anomalous subdiffusion adaptation of Eq. 6 yields $\alpha = 0.55 \pm 0.10$, $D(10\ \mu s) = 9.2 \pm 3.7 \times 10^{-7}\ cm^2s^{-1}$, $D(6\ ms) = 5.3 \pm 2.0 \times 10^{-8}\ cm^2s^{-1}$.

DISCUSSION

These experiments have demonstrated the utility of MP-FPR in the measurement of the 3D diffusion coefficient of fluorescent species in bulk solutions and in living cells. The correct 3D diffusion coefficient of wild-type GFP in aqueous solution was measured with a 3D resolution of a few microns within a much larger volume of solution. This suggests that the theoretical analysis presented above correctly describes the behavior of freely diffusing systems probed with multiphoton excited photobleaching.

In the cytoplasm of living cells a slight enhancement of the MP-FPR free-diffusion analysis may be required to fit in vivo recovery curves. Diffusive recovery of calcein in RBL cells is well described by an anomalous subdiffusion model with $\langle r^2 \rangle = \Gamma t^{\alpha}$. The resultant value of the anomalous subdiffusion parameter, $\alpha = 0.55 \pm 0.1$, suggests that weak potential energy traps, such as sites of transient binding to the immobile cytoplasmic matrix or to less mobile cytoplasmic proteins, have a significant impact on the diffusivity of this species in vivo. This experiment demonstrates the importance of unconventional diffusion mechanisms such as anomalous subdiffusion, anomalous superdiffusion, or continuous distributions of diffusion coefficients in the understanding of diffusive processes in living cells and in the treatment of in vivo MP-FPR data. Similar evidence for anomalous subdiffusion in cellular cytoplasm has been found by FCS measurements (Petra Schwille and Watt Webb, private communication).

It is appropriate to consider whether 3D FPR can be accomplished by one-photon excitation. It has been claimed without experimental evidence (Blonk et al., 1993) that one-photon excited photobleaching with confocal detection can yield the 3D diffusion coefficient of fluorophores with 3D resolution. This one-photon experiment is faced with the general problem that the axial extent of the spreading double cone of the bleaching distribution will be dependent upon the sample thickness and may be unknown. This double cone of bleached molecules will diffuse into and out of the confocal volume, thereby affecting the recovery curve

in a manner dependent upon the diffusive properties of the environment outside of the focal volume as well as the boundary conditions. In Blonk et al. this difficulty is ignored and the bleaching distribution generated by one-photon excitation is approximated as a Gaussian in three dimensions. As discussed above, the radially integrated fluorescence excitation and thus the photobleaching is in fact constant at each position along the optical axis under one-photon excitation, and the total bleaching does not decrease axially along a Gaussian profile. Consequently, this approximation neglects the fact that the characteristic radial width of the bleaching distribution generated by one-photon excitation becomes larger above and below the focal plane and has an axial extent defined by the sample thickness.

Based upon these considerations one would predict that the diffusion coefficients reported by this methodology would be erroneously small and that the error would increase as the numerical aperture (NA) of the objective increased. We applied the treatment of Blonk et al. for one-photon confocal FPR to the measurement of the diffusion of 40 kDa dextrans in water near ($\sim$10–40 μm) the coverslip of a large sample volume and found that the diffusion coefficient reported by this methodology was incorrectly low by more than a factor of 10 at 0.5 NA, and the error increases to a factor of 50 as the NA increases from 0.5 to 1.33 (data not shown). Note that the MP-FPR recovery curves derived above are equivalent to the open-aperture, no scanning limit of the formulas derived by Blonk et al. (1993) because of their use of a 3D Gaussian approximation to the one-photon excitation distribution.

MP-FPR error analysis

Systematic error

The primary sources of systematic error in MP-FPR experiments are excessive monitoring or bleaching powers, overly long bleaching flashes or time bins, and reversible photobleaching of the fluorophore. All of these errors can be avoided with proper care, as discussed below.

Systematic error: average photobleaching power

The maximum allowed average photobleaching power at the sample P_b is limited by the assumption inherent in Eq. 2 that the rate of excitation of fluorophores undergoing b-photon excitation (and subsequent photobleaching) is directly proportional to the bth power of the excitation light intensity for all excitation intensities. This is not true at such high excitation intensities that the fluorophores might undergo ground-state depletion (saturation). The kinetics of saturation using pulsed illumination (Xu and Webb, 1997) differ from continuous illumination (Sandison et al., 1995). Fluorescence lifetimes are much longer than the Ti:sapphire pulse duration (ns versus fs) and usually shorter than the period between pulses ($\sim$12 ns). As a result, the maximum possible rate of excitation of fluorophores with pulsed lasers is the repetition rate of the laser ($\sim$80 MHz for commercially available Ti:sapphire lasers). Intersystem crossing may further decrease the maximum useful excitation rate.

Taking ground-state depletion into account and approximating the laser pulse train as a sequence of pulses of Gaussian temporal profile with average intensity $\langle I_{bl}, (r, z)\rangle$, temporal width τ, and repetition rate ω, Eq. 3 (the concentration distribution of unbleached fluorophores after a laser pulse train of duration Δt) becomes

$$c(r, z, t = \Delta t) = c_0(1 - q_b(1 - e^{-(1/b)g_p^{(b)}\delta\langle I_{bl}(r,z)\rangle^b\omega^{-b}\tau^{1-b}}))^{\omega\Delta t} \quad (12)$$

where $g_p^{(b)}$ is a measure of the bth order temporal coherence of the laser pulse (Xu and Webb, 1997). This expression is only equivalent to Eq. 3 for small values of the saturation parameter $s = (1/b)g_p^{(b)}\delta\langle I_{bl}(r, z)\rangle^b\omega^{-b}\tau^{1-b}$, which in this limit represents the excitation probability of a single molecule during an individual laser pulse. While Eq. 12 is more general than Eq. 3, the derivation of MP-FPR curves using this expression for the initial fluorophore concentration distribution is mathematically burdensome, and consequently MP-FPR is performed in the nonsaturated regime, using Eq. 3. This sets an upper limit on the allowed central photobleaching intensity.

The maximum photobleaching power before excitation saturation can be determined experimentally by measuring the bleach depth parameter β as a function of the average photobleaching power. The results of such a saturation study can be observed in Fig. 3, where MP-FPR was performed with a series of high bleaching intensities on aqueous solutions of wild-type GFP. In this demonstration a 1.3-NA objective was only minimally overfilled (the e^{-1} beam waist is equal to the radius of back aperture) to deliver the maximum power to the focal volume. In Fig. 3, β scales as power squared at low bleaching powers, indicating a two-photon bleaching process and a value of $b = 2$. This confirms that Eq. 2 is a valid model for photobleaching in this power range. At higher powers, β falls from a quadratic dependence on the average photobleaching power as a significant fraction of fluorophores are excited by each laser pulse.

The apparent onset of saturation is marked with a vertical line in Fig. 3, which corresponds to a power at the sample of $\sim$44 mW and a calculated value of s $\sim$ 1, assuming a two-photon action cross section of 6 GM at 780 nm (Xu et al., 1996), fluorescence quantum efficiency of 0.86 (Palm et al., 1997), and a second-order temporal coherence factor of $g_p^{(2)} = 0.66$ (Xu and Webb, 1997). At this level of saturation ($s = 1$), the photobleaching parameter is $\sim$13% smaller than expected. This is in close agreement with a previous theoretical prediction that under two-photon excitation conditions where the saturation parameter is equal to 1 there will be a $\sim$13% loss of fluorescence signal (Xu and Webb, 1997). Consequently, Fig. 3 demonstrates that MP-FPR

experiments on wild-type GFP should be restricted to values of s less than ~1 to avoid saturation. In our experiment, this saturation limit manifested itself as a requirement that we restrict our average photobleaching powers to less than ~44 mW at the sample. The motivation for avoiding saturation is clear from another result of this series of preliminary MP-FPR experiments; diffusion coefficients calculated from fits to data taken well into the saturated regime of Fig. 3 were as low as ~70% of the values taken from data in the unsaturated regime.

Some fluorophores have been shown to photobleach via excited-state absorption at high excitation intensities (Brand et al., 1997; Eggeling et al., 1997). These complex photobleaching kinetics should reveal themselves as a deviation from the appropriate relationship between bleach depth and excitation power (i.e., a deviation from the power squared relationship of two-photon photobleaching) and can be avoided by the same technique described above for the avoidance of excitation saturation.

With sufficient computing power it may be possible to perform accurate MP-FPR experiments at high bleaching powers, well into the saturation regime. The motivation for this would be to increase the bleach depth and thereby improve the signal-to-noise ratio of a single bleach/monitor sequence. This would involve the use of Eq. 12 in place of Eq. 3, and the numerical integration of the resultant diffusive recovery and fluorescence signal integrals. This would also involve the independent measurement of q_b, the quantum efficiency of photobleaching, or its inclusion as an independent fitting parameter. While saturating photobleaching powers may be a viable alternative in certain experiments, a few possible problems need to be explored before this is attempted in a given system. One possible problem with saturating bleach powers is the likelihood that MPE-induced photodamage exhibits a threshold effect (Nichols et al., 1998), whereby excitation doses below a certain threshold generate no distinguishable cellular damage, while doses above a certain threshold initiate cellular damage or even cell death. Another possible problem is the occurrence of higher order photobleaching processes, as discussed above. The significance of these processes will need to be quantified by using bleach depth versus power measurements similar to those in Fig. 3, fitting the resultant data to the expected bleach depth with saturation, and verifying that there are no systematic deviations due to higher order processes. A third possible problem is the relatively low fluorescence signal in the crucial early phase of the recovery, which will be entailed by extremely deep bleaches. If these difficulties are overcome, then saturating photobleaching powers may become a useful tool.

Systematic error: average monitoring power

The maximum allowed monitoring power in a MP-FPR experiment is limited by the need to avoid photobleaching. Equation 3 assumes that photobleaching occurs only over the duration Δt of the photobleaching pulse, and not during the monitoring period before or after this pulse. While some photobleaching will always occur when fluorescence is generated, the amount of photobleaching generated during the monitoring period of an MP-FPR experiment can be rendered experimentally insignificant relative to the amount generated during the photobleaching pulse by limiting the maximum monitoring power used. The maximum allowed monitoring power can be determined by turning off the bleaching pulse and verifying that the signal generated by the monitoring beam does not decrease noticeably over the time course of the experiment relative to the shot noise in the data (i.e., $F(t)$ is a straight line with a slope of 0). In the MP-FPR experiments described above the maximum average monitoring power was restricted to levels where no significant photobleaching was generated by the monitoring beam. To improve the signal-to-noise ratio it is always possible to pulse the monitoring beam to high intensities, where measurable bleaching is generated, as long as the bleaching introduced by these monitoring pulses is not a significant fraction of the bleaching introduced by the primary bleaching pulse.

Systematic error: duration of photobleaching flash and time bins

The maximum allowed duration of the photobleaching pulse Δt and the length of the time bins t_{bins} in an FPR experiment are dictated by the need to avoid significant fluorophore diffusion during the pulse and to accurately record the resultant recovery curve. Equation 3 assumes that no significant diffusion occurs during the bleaching pulse, and using Eq. 6 for analysis of MP-FPR curves will yield incorrectly small diffusion coefficients if the duration of the uncaging pulse is long enough to allow significant fluorophore diffusion. Likewise, accurate measurement of the resultant fluorescence recovery curve requires that no significant diffusion occurs within the space of a single time bin, and this is most crucial during the early, rapidly changing portion of the recovery curve. The fractional error in the recorded fluorescence signal, generated by diffusive recovery during Δt (or t_{bins}), can be estimated by calculating the amount of diffusionally generated fluorescence recovery expected during this interval (equal to the initial slope of the recovery curve, given by Eq. 8, times Δt or t_{bins}) and dividing by the bleach depth (Eq. 7). This is given by

$$\frac{\partial F/\partial t|_{t=0}\Delta t}{\Delta F} = \frac{\Delta t}{\tau_D}\left(\frac{1}{2R} + 1\right)\frac{b}{2}\left[e^{-\beta/11.7}\right] \qquad (13)$$

where the term in square brackets is an approximation valid for $\beta = 0-4$. In this expression Δt can represent either the bleach pulse duration Δt or the duration of the time bins t_{bins}. In the first case the reported fractional error in $F(t)$ then represents the error due to diffusive recovery during the bleaching pulse, while in the second case the reported fractional error in $F(t)$ then represents the error due to diffusive recovery during overly long time bins. In our

experiments with wtGFP, $R \approx 3$, $b = 2$, and the bleach depth parameter was on the order of 1 or less. This systematic error in $F(t)$ is therefore expected to be $\sim 1.05(\Delta t/\tau_D)$. We found that the characteristic fluorescence recovery time was ~ 200 μs (see Fig. 4). Consequently, a bleaching pulse length of 7.2 μs was short enough to avoid significant diffusion during the pulse (error in $F(t)$ of $\sim 4\%$), and $t_{bins} = 10.24$ ms was short enough to accurately follow the fluorescence recovery curve (error in $F(t)$ of $\sim 5\%$).

Systematic error: reversible photobleaching

Previous one-photon FPR studies of the S65T mutant of GFP have reported significant nondiffusive recovery in fluorescence after photobleaching (referred to as "reversible photobleaching") with a millisecond recovery time (Swaminathan et al., 1997). The presence of significant reversible photobleaching kinetics on the same time scales as the diffusional transit of a fluorophore through the multiphoton focal volume may contribute a diffusion-independent component to the detected signal recovery after a photobleaching pulse train. This may generate a systematic error in the diffusion coefficients reported.

FCS studies of EGFP have revealed pH-dependent spontaneous loss and recovery of fluorescence with a 200-μs time scale and triplet state blinking with similar or shorter time scales (Maiti et al., 1998). Similar work with fluorescein has also reported reversible photobleaching due to triplet state relaxation, although with a microsecond recovery time (Periasamy et al., 1996). To investigate possible millisecond time scale photochemical fluorescence recovery in wild-type GFP, MP-FPR was performed, using 250-μs pulse trains of 790 nm light focused with a drastically underfilled 1.3 NA objective (e^{-1} beam waist $\ll$ radius of the back aperture of the objective) to enlarge the focal volume in a viscous 90% glycerol solution containing wild-type green fluorescent protein diluted to 3.7 μM. The resultant time course of the fluorescence signal was accumulated using 40-μs time bins. The addition of glycerol and the underfilling of the objective lens served to slow the diffusional fluorescence recovery signal and separate it in time from possible millisecond fluorescence recovery due to reversible photobleaching. Underfilling the lens prevents the accurate application of Eq. 6 to the system by invalidating the ellipsoidal Gaussian approximation, but allows for the detection of reversible photobleaching. No significant reversible photobleaching in wild-type GFP was observed with a half-recovery time in the ~ 200 μs to ~ 8 ms range. Any reversible component of the photobleaching was restricted to less than 10% of the total bleach depth for bleaching powers up to ~ 100 mW at the sample.

These results suggest that MP-FPR can be performed on aqueous solutions of wild-type GFP with diffusional recovery times in the ~ 200 μs to ~ 8 ms regime without any transiently nonfluorescent states contributing to significant systematic errors in D.

In these experiments, the possibility of reversible photobleaching was probed as described previously before accurate diffusion coefficient measurements were attempted. These steps should be considered for all FPR experiments, on each fluorescent marker used. If tests for reversible photobleaching do reveal a significant reversible component in a given experimental system, it may still be possible to measure diffusion coefficients accurately. If the reversible fluorescence is due to excitation into a triplet state (as may be the case for S65T GFP at high intensity), then limitation of the photobleaching pulse to lower intensities may limit the amount of fluorophore pumped into this state while still producing enough bleach for accurate diffusion coefficient determination. If significant reversible photobleaching is unavoidable even at the lowest photobleaching powers allowed for accurate diffusion coefficient determination, it may still be possible to measure accurate diffusion coefficients, depending upon the relative time scales of the photochemical versus diffusive fluorescence recovery.

If the recovery time scale of reversible photobleaching is significantly longer than that of diffusional recovery, the derivations leading to Eq. 6 remain valid. The definition of bleaching used in this work includes transitions into any nonfluorescent state whose lifetime is significantly longer than the diffusive recovery of the system, allowing for the presence of reversible photobleaching, which recovers over sufficiently slow time scales. To push a given experimental system farther into this regime the diffusion times can be lowered by using higher numerical aperture optics and a shorter excitation wavelength. As has been addressed above, if the time scale of reversible fluorescence recovery is on the same time scale as diffusional recovery, Eq. 6 loses its validity, and it becomes problematic to derive diffusion coefficients without a far more rigorous treatment of the various reacting and diffusing populations of molecules. If the time scale of reversible recovery is significantly faster than the diffusive recovery, the use of Eq. 6 to derive diffusion coefficients is again valid, as the fast recycling through the reversible state will only affect the effective quantum efficiency of photobleaching. Accurately measured diffusion coefficients have been reported using conventional FPR in just such a complex system (Swaminathan et al., 1997).

Random error

The primary source of random error in MP-FPR experiments is shot noise in the recorded fluorescence signal. Constraints on the maximum allowed duration of the time bins and the maximum allowed average monitoring power limit the maximum fluorescence signal that can be detected with a given MP-FPR instrument in a single pulse-monitor sequence. Constraints on the maximum average bleaching power and the duration of the bleach pulse Δt set the maximum value of the bleach depth parameter β that can be achieved with a given fluorophore and excitation optics. Altogether, these constraints limit the signal-to-noise ratio

in a given experiment and can necessitate averaging of many consecutive pulse-monitoring sequences to achieve values of the diffusion coefficient with a desired accuracy.

The scaling of the expected uncertainty in the diffusion coefficient with the aforementioned parameters can be calculated beginning with the realization that the relative uncertainty in the value of the diffusion coefficient $\Delta D/D$ produced by an MP-FPR experiment is proportional to the relative uncertainty in the calculated diffusion time, $\Delta\tau_D/\tau_D$. The relative uncertainty in the calculated diffusion time can then be estimated from the relative uncertainty or "noise" in the detected fluorescence signal $\Delta F(t)/F(t)$ by evaluating the derivative of Eq. 6 at $t = \tau_D$. To gain physical insight into the sources of uncertainty in this experiment without getting lost in mathematical detail, we do not evaluate the derivative of the full infinite series in Eq. 6, but take the limit that β is small ($\beta < 0.1$) and find that the relative uncertainty in the calculated diffusion coefficient is approximately

$$\frac{\Delta D}{D} \sim \frac{1}{\beta\sqrt{St_{bin}N}} \tag{14}$$

where we have also assumed that the noise in the fluorescence recovery signal after the photobleaching pulse is approximately equal to the noise in the steady-state fluorescence signal and that this noise is due to Poisson statistics ("shot noise"). S is the detected count rate, t_{bin} is the length of the time bins used to record this detected signal, and N is the number of successive bleach/monitor sequences that are summed to improve the signal-to-noise ratio. The detected count rate S is proportional to three readily accessible experimental parameters: E, the overall detection efficiency; $\langle I^m_{mo}\rangle$, the average monitoring intensity; and c_0, the equilibrium concentration of the fluorophore.

This expression reveals how the various experimental constraints described in the Systematic Error section contribute to the number of averages N required to achieve a minimum relative uncertainty $\Delta D/D$. The bleach depth is limited by excitation saturation, and the duration of the time bins is limited by the diffusion time of the fluorophore through the focal volume chosen for the experiment. This leaves the rate of fluorescence detection S and the number of averages N as the relevant free parameters left that can be adjusted to attain a desired signal-to-noise ratio.

These two parameters are not entirely free, however. The detected count rate S is proportional to the monitoring intensity $\langle I^m_{mo}\rangle$, the overall efficiency of detection E, and the equilibrium concentration of fluorophores c_0. The monitoring intensity is constrained by the need to avoid photobleaching, the detection efficiency is dictated by the available technology and choice of optics, and the fluorophore concentration will often be dictated by the biological properties of the system being studied. Once these last two parameters are optimized, the number of averages N is left as the last parameter that can be freely varied to improve the signal-to-noise ratio.

As a specific example, in the GFP experiments described above, 4.4 μM GFP diffusing freely through a focal volume generated by a 1.33-NA overfilled objective was monitored close to the maximum fluorescence detection rate allowed by negligible photobleaching and the detection system described in the Materials and Methods section. The relatively low concentration of fluorophore was bleached to a value of the bleach depth parameter close to the limit given by excitation saturation and diffusion of the fluorophore and required 10,000 consecutive bleach/pulse protocols to yield diffusion coefficients of ~20% relative certainty (standard deviation of 22 trials divided by the mean). From Eq. 14 we can predict that if fewer averages were desired while maintaining the same certainty in D, the diffusion time and consequently the allowed bleach pulse and time bin duration could be lengthened by lowering the NA of the objective. However, this would degrade the spatial resolution of the experiment. Alternatively, as these experiments were performed in vitro, the concentration of fluorophore could easily be increased. A concentration of 1 mM GFP would only need ~44 averages to yield the same uncertainty in D when excited at 780 nm, but these high concentrations may not be attainable in biological samples. In general, the limitations set by excitation saturation, photobleaching, the efficiencies of detection schemes, and rapid diffusion time scales will often necessitate a number of averages of the bleach/monitor protocol to achieve a good signal-to-noise ratio.

In the in vitro aqueous GFP demonstration experiment carried out above, the multiple averaging dictated by the low fluorophore concentration had no ill effects. In a living cell, however, multiple high-intensity bleaching flashes may cause concern because of the possibility of photodamage. The in vivo experiment described above used 50 flash/monitor sequences to derive the diffusion coefficient of calcein in RBL cells, with no visible ill effect on the cell studied. While the effect of multiple flashes should be evaluated for each biological system studies, this demonstrates that in principle, MP-FPR with multiple flashes can be successfully applied in vivo.

The necessity for multiple flashes may also be of concern when there is a high probability that a certain fraction of the fluorophore will be effectively immobile. In a MP-FPR experiment where only one pulse-monitoring sequence is used, an immobile fraction will be revealed if the asymptotic value of the post-bleach fluorescence, $F(\infty)$, is less than the equilibrium fluorescence signal before the bleaching pulse, F_0. The fraction of fluorophore that is immobile is then given by

$$\frac{F_0 - F(\infty)}{F_0 - F(0)} \tag{15}$$

In experiments utilizing multiple bleach-monitor sequences, this immobile fraction should generally be completely photolyzed after the first few bleach pulses, and ensuing bleach-monitor sequences will detect no immobile fraction. The

final MP-FPR curve should therefore greatly underrepresent the immobile fraction or not reveal it at all (i.e., $F(\infty)$ will be equal to F_0 within the noise in the data). It is important to note that this "transparency" to the immobile fraction of those MP-FPR experiments that require multiple sequence averaging should not significantly affect the reported D of the mobile fraction. Furthermore, the value of the immobile fraction can be directly measured by drastically increasing the duration of the time bins of the experiment (allowing greater averaging per bin) and performing a single bleach monitor sequence.

CONCLUSION

In this work we have provided a guide to the use of MP-FPR in the measurement of 3D diffusion coefficients of fluorophores in solution, accompanied by the demonstration of the accuracy and applicability of this new method on aqueous solutions of wild-type GFP. We have described the limitations to this technique presented by such effects as excitation saturation, photobleaching during fluorescence detection, and reversible photobleaching and demonstrated how to determine these limitations experimentally. We find that MP-FPR can measure the 3D diffusion coefficient of wild-type GFP in water ($D = 8.7\ \mathrm{cm^2 s^{-1}}$) at only 4.4 μM concentration with $\pm 20\%$ uncertainty and a spatial resolution of a few microns, using multiple flash/monitor sequences averaged over ~8 min. Higher concentrations of fluorophore will allow correspondingly shorter averaging times. We have also demonstrated the applicability of MP-FPR inside living cells. We find that the MP-FPR curves produced with 50 bleach/monitor repetitions performed over 10 s on calcein at ~100 μM in the cytoplasm of RBL-2H3 cells are well fit by an anomalous subdiffusion model $D(t) = \Gamma t^{\alpha-1}$ with $\alpha = 0.55 \pm 0.10$, $D(10\ \mu\mathrm{s}) = 9.2 \pm 3.7 \times 10^{-7}\ \mathrm{cm^2 s^{-1}}$, and $D(6\ \mathrm{ms}) = 5.3 \pm 2.0 \times 10^{-8}\ \mathrm{cm^2 s^{-1}}$.

We have also experimentally evaluated the applicability of confocal one-photon FPR to 3D diffusion geometries. We find that the extended double cone of bleached fluorophore generated by one-photon excitation prevents confocal one-photon FPR from determining accurate 3D diffusion coefficients with significant 3D resolution.

With the accurate measurement of the known diffusion coefficient of wild-type GFP in aqueous solution, we have demonstrated how, if proper excitation conditions are used, this technique can produce 3D diffusion coefficients with a spatial resolution of a few microns. The MP-FPR theory and techniques presented here can therefore be used in a variety of diffusional measurements that require 3D resolution. It can be utilized in thick tissue samples to explore local viscosity domains in cells or used to probe the 3D diffusive transport of biological molecules within the cytoplasm of cells or within intracellular spaces.

APPENDIX

The initial concentration distribution of unbleached fluorophores immediately after the cessation of the photobleaching pulse train is given by

$$c(r, z, t = 0) = c_0 \exp[-(1/b) q_b \delta \langle I_{bl}^b(r, z)\rangle \Delta t] \qquad \text{(I)}$$

where the end of the photobeaching pulse train is now defined as $t = 0$ and the spatial distribution of the excitation beam is given by the ellipsoidal Gaussian approximation:

$$\langle I_{bl}^b(r, z)\rangle = \langle I_{bl}^b(0, 0)\rangle \exp\left[-\frac{2br^2}{w_r^2} - \frac{2bz^2}{w_z^2}\right] \qquad \text{(II)}$$

The temporal behavior of this nonequilibrium concentration distribution can be calculated by using the integral form of the diffusion equation:

$$c(r, z; t) = \int G(r, z, r', z'; t) c(r', z'; 0) 2\pi r'\, dr'\, dz' \qquad \text{(III)}$$

where $G(r, z, r', z'; t)$ is the Green's function of the diffusion equation in cylindrical coordinates, given by

$$G(r, z, r', z'; t) = \frac{I_0(rr'/2Dt)}{(4\pi Dt)^{3/2}} \exp\left[-\frac{r^2 + r'^2 + (z - z')^2}{4Dt}\right] \qquad \text{(IV)}$$

where I_0 is the modified Bessel function of the first kind. Substituting Eqs. IV and I into Eq. III and using the series expansion of the exponential function in Eq. I yields the time-dependent concentration distribution of unbleached fluorophore after the end of the photobleaching pulse train:

$$c(r, z; t) = c_0 \sum_{n=0}^{\infty} \frac{(-\beta)^n \exp\left[-\frac{2bnz^2}{w_z^2}\frac{1}{1 + (8bnDt/w_z^2)} - \frac{2bnr^2}{w_r^2}\frac{1}{1 + (8bnDt/w_r^2)}\right]}{n!(1 + (8bnDt/w_z^2))^{1/2}(1 + (8bnDt/w_r^2))} \qquad \text{(V)}$$

where $\beta \equiv (1/b) q_b \delta \langle I_{bl}^b(0, 0)\rangle \Delta t$ is the bleaching depth parameter. This concentration distribution is then monitored by the same laser beam that produced the photobleaching pulse train, albeit greatly attenuated. The fluorescent signal detected is then given by

$$F(t) = (1/m) \delta_m E \int \langle I_{mo}^m(r, z)\rangle c(r, z, t) 2\pi r\, dr\, dz \qquad \text{(VI)}$$

where $\langle I_{mo}^m(r, z)\rangle$ is the time average of the monitoring intensity raised to the mth power, m is the number of photons required to generate fluorescence from the fluorophore, and δ_m is the multiphoton fluorescence action cross section. Equation V can be inserted into Eq. VI to produce this time-dependent detected fluorescence signal:

$$F(t) = F_0 \sum_{n=0}^{\infty} \frac{m^{3/2}(-\beta)^n}{n!} \frac{1}{(m + bn + (bnmtD/w_r^2))} \times \frac{1}{\sqrt{m + bn + (bnmtD/w_z^2)}} \qquad \text{(VII)}$$

where F_0 is the equilibrium fluorescence signal detected during the monitoring phase, before the photobleaching pulse train.

This work was carried out at the Developmental Resource for Biophysical Imaging and Optoelectronics, with funding provided by the National Science Foundation (grant DIR 88002787) and the National Institutes of Health (NIH) (grants RR07719 and RR0422). The basic theoretical analysis was devised by EW in 1992 during a sabbatical in the Webb laboratory at Cornell (Piston et al., 1992); the development of practical experimental procedures, testing, and tractable analysis was carried out by EBB, who was supported as a predoctoral trainee under NIH grant T32GM09267, and WZ tested the technique in vivo and tested the one-photon confocal alternative technique.

REFERENCES

Axelrod, D., D. Koppel, J. Schlessinger, E. Elson, and W. Webb. 1976. Mobility measurement by analysis of fluorescence photobleaching recovery kinetics. *Biophys. J.* 16:1055–1069.

Berland, K., P. So, and E. Gratton. 1995. Two-photon fluorescence correlation spectroscopy: method and application to the intracellular environment. *Biophys. J.* 68:694–701.

Blonk, J., A. Don, H. Van Aalst, and J. Birmingham. 1993. Fluorescence photobleaching recovery in the confocal light scanning microscope. *J. Microsc.* 169:363–374.

Born, M., and E. Wolf. 1983. Principles of Optics, 6th Ed. Pergamon Press, New York.

Bouchard, J., and A. Georges. 1990. Anomalous diffusion in disordered media; statistical mechanisms, models and physical applications. *Phys. Rep.* 195:127–293.

Brand, L., C. Eggeling, C. Zander, K. Drexhage, and C. Seidel. 1997. Single-molecule identification of coumarin-120 by time-resolved fluorescence detection: comparison of one- and two-photon excitation in solution. *J. Phys. Chem. A.* 101:4313–4321.

Cherry, R. 1979. Rotational and lateral diffusion of membrane proteins. *Biochim. Biophys. Acta.* 559:289–327.

Denk, W., D. Piston, and W. Webb. 1995. Two-photon molecular excitation in laser-scanning microscopy. *In* Handbook of Biological Confocal Microscopy. J. Pawley, editor. Plenum Press, New York. 445–457.

Edidin, M., M. Zagyansky, and T. Lardner. 1976. Measurement of membrane protein lateral diffusion in single cells. *Science.* 191:466–468.

Eggeling, C., L. Brand, and C. Seidel. 1997. Laser-induced fluorescence of coumarin derivatives in aqueous solution: photochemical aspects for single molecule detection. *Bioimaging.* 5:105–115.

Feder, T., I. Brust-Mascher, J. Slattery, B. Baird, and W. Webb. 1996. Constrained diffusion or immobile fraction on cell surfaces: a new interpretation. *Biophys. J.* 70:2767–2773.

Ghosh, R., and W. Webb. 1988. Results of automated tracking of low density lipoprotein receptors on cell surfaces. *Biophys. J.* 53:352a.

Henkel, A., L. Simpson, R. Ridge, and W. Betz. 1996. Synaptic vesicle movements monitored by fluorescence recovery after photobleaching in nerve terminals stained with FM1–43. *J. Neurosci.* 16:3960–3967.

Johnson, E., D. Berk, R. Jain, and W. Deen. 1996. Hindered diffusion in agarose gels: test of effective medium model. *Biophys. J.* 70:1017–1023.

Kasche, V., and L. Lindqvist. 1964. Reactions between the triplet state of fluorescein and oxygen. *J. Phys. Chem.* 68:817–823.

Luby-Phelps, K., D. Taylor, and F. Lanni. 1986. Probing the structure of cytoplasm. *J. Cell Biol.* 102:2015–2022.

Maiti, S., U. Haupts, P. Schwille, and W. Webb. 1998. Kinetics of chromophore protonation in EGFP determined by fluorescence correlation spectroscopy. *Biophys. J.* 74:A274.

Mertz, J., C. Xu, and W. Webb. 1995. Single-molecule detection by two-photon excited fluorescence. *Opt. Lett.* 20:2532–2534.

Nichols, J., and W. Webb. 1998. Multiphoton microscopy: a tool to study photodamage. *FASEB J.* 12(S):A497.

Palm, G., A. Zdanov, G. Gaitanaris, R. Stauber, G. Pavlakis, and A. Wlodawer. 1997. The structural basis for spectral variations in green fluorescent protein. *Nature Struct. Biol.* 4:361–365.

Periasamy, N., S. Bicknese, and A. Verkman. 1996. Reversible photobleaching of fluorescein conjugates in air-saturated viscous solutions: singlet and triplet state quenching by tryptophan. *Photochem. Photobiol.* 63:265–271.

Periasamy, N., and A. S. Verkman. 1998. Analysis of fluorophore diffusion by continuous distributions of diffusion coefficients: applications of photobleaching measurements of multicomponent and anomalous diffusion. *Biophys. J.* 75:557–567.

Peters, R., J. Peters, K. Tews, and W. Bahr. 1974. Microfluorimetric study of translational diffusion of proteins in erythrocyte membranes. *Biochim. Biophys. Acta.* 367:282–294.

Piston, D., E. Wu, and W. Webb. 1992. Three dimensional diffusion measurements in cells by two-photon excitation fluorescence photobleaching recovery. *Biophys. J.* 61:A34.

Press, W., S. Teukolsky, W. Vettering, and B. Flannery. 1992. Numerical Recipes in C. Cambridge University Press, New York.

Sandison, D., R. Williams, K. Wells, J. Strickler, and W. Webb. 1995. Quantitative fluorescence confocal laser scanning microscopy (CLSM). *In* Handbook of Biological Confocal Microscopy. J. Pawley, editor. Plenum Press, New York. 445–457.

Schlessinger, J., D. Koppel, D. Axelrod, K. Jacobson, W. Webb, and E. Elson. 1976. Lateral transport on cell membranes: mobility of concavalin A receptors on myoblasts. *Proc. Natl. Acad. Sci. USA.* 73: 2409–2413.

Song, L., E. Hennink, T. Young, and H. Tanke. 1995. Photobleaching kinetics of fluorescein in quantitative fluorescence microscopy. *Biophys. J.* 68:2588–2600.

Song, L., C. Varma, J. Verhoeven, and H. Tanke. 1996. Influence of the triplet excited state on the photobleaching kinetics of fluorescein in microscopy. *Biophys. J.* 70:2959–2968.

Svoboda, K., D. Tank, and W. Denk. 1996. Direct measurement of coupling between dendritic spines and shafts. *Science.* 272:716–719.

Swaminathan, R., S. Bicknese, N. Periasamy, and A. Verkman. 1996. Cytoplasmic viscosity near the cell plasma membrane: translational diffusion of a small fluorescent solute measured by total internal reflection-fluorescence photobleaching recovery. *Biophys. J.* 71:1140–1151.

Swaminathan, R., C. Hoang, and A. Verkman. 1997. Photobleaching recovery and anisotropy decay of GFP-S65T in solution and cells: cytoplasmic viscosity probed by GFP translational and rotational diffusion. *Biophys. J.* 72:1900–1907.

Wedekind, P., U. Kubitscheck, and R. Peters. 1997. 3D diffusion measured at high spatial and temporal resolution by scanning microphotolysis. *Biophys. J.* 72:A245.

Xu, C., W. Zipfel, J. Shear, R. Williams, and W. Webb. 1996. Multiphoton fluorescence excitation: new spectral windows for biological nonlinear microscopy. *Proc. Natl. Acad. Sci. USA.* 98:10763–10768.

Xu, C., and W. Webb. 1997. Multiphoton excitation of molecular fluorophores and nonlinear laser microscopy. *In* Topics in Fluorescence Spectroscopy, Vol. 5: Nonlinear and Two-Photon Induced Fluorescence. J. Lackowicz, editor. Plenum Press, New York. 471–540.

Yguerabide, J., J. Schmidt, and E. Yguerabide. 1982. Lateral mobility in membranes as detected by fluorescence photobleaching recovery. *Biophys. J.* 39:69–75.